ACS OMEGA

Open Access

http://pubs.acs.org/journal/acsodf

Article

Cholesterol and Ceramide Facilitate Membrane Fusion Mediated by the Fusion Peptide of the SARS-CoV-2 Spike Protein

Kristina Niort, Julia Dancourt, Erwan Boedec, Zahra Al Amir Dache, Grégory Lavieu, and David Tareste*

Cite This: *ACS Omega* 2023, 8, 32729−32739

Read Online

ACCESS | Metrics & More | Article Recommendations | Supporting Information

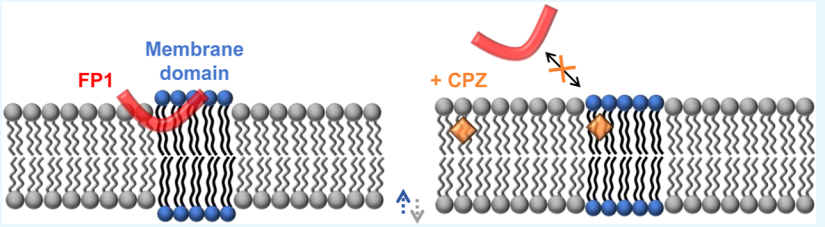

ABSTRACT: SARS-CoV-2 entry into host cells is mediated by the Spike (S) protein of the viral envelope. The S protein is composed of two subunits: S1 that induces binding to the host cell *via* its interaction with the ACE2 receptor of the cell surface and S2 that triggers fusion between viral and cellular membranes. Fusion by S2 depends on its heptad repeat domains that bring membranes close together and its fusion peptide (FP) that interacts with and perturbs the membrane structure to trigger fusion. Recent studies have suggested that cholesterol and ceramide lipids from the cell surface may facilitate SARS-CoV-2 entry into host cells, but their exact mode of action remains unknown. We have used a combination of *in vitro* liposome−liposome and *in situ* cell−cell fusion assays to study the lipid determinants of S-mediated membrane fusion. Our findings reveal that both cholesterol and ceramide lipids facilitate fusion, suggesting that targeting these lipids could be effective against SARS-CoV-2. As a proof of concept, we examined the effect of chlorpromazine (CPZ), an antipsychotic drug known to perturb membrane structure. Our results show that CPZ effectively inhibits S-mediated membrane fusion, thereby potentially impeding SARS-CoV-2 entry into the host cell.

INTRODUCTION

Cellular infection by SARS-CoV-2 starts with the fusion of its lipid envelope with the host cell membrane leading to the delivery of its genomic RNA into the cell cytoplasm. Such a fusion event can occur directly with the cell plasma membrane or with the endosomal membrane following the endocytosis of SARS-CoV-2. Several lines of evidence obtained with SARS-CoV-2 or the closely related coronaviruses SARS-CoV and MERS-CoV suggest that direct fusion with the plasma membrane is the preferred route, notably during infection of the respiratory cells.[1−6] Because it occurs early in the viral replication cycle, this early fusion step is an attractive target for the development of drugs and vaccines that are able to block virus entry.[7]

SARS-CoV-2 binding and fusion with the cell membrane is mediated by the Spike (S) protein, a class I viral fusion protein composed of two subunits, S1 and S2. The S1 subunit is involved in binding to the host cell plasma membrane *via* its interaction with the human angiotensin-converting enzyme (ACE2) receptor of the cell surface,[8−10] whereas the S2 subunit mediates the fusion of the SARS-CoV-2 lipid envelope with the host cell membrane.[11] For the S2 subunit to be available for fusion, the S protein must be cleaved at the S1/S2 interface by cellular proteases after S1 binding to ACE2.[6,12]

The S2 subunit of the SARS-CoV-2 S protein possesses an N-terminal fusion peptide (FP), followed by two heptad repeat domains (HR1 and HR2), and a transmembrane domain (TMD) that anchors the S protein into the viral membrane. Fusion by S2 starts with the insertion of its FP into the target cell membrane to establish a molecular bridge consisting of a three-helix coiled-coil complex composed of its HR1 and HR2 domains. S2 then folds back onto itself, in the form of a six-helix coiled-coil hairpin complex of the HR1 and HR2 domains, which brings the FP and TMD in molecular proximity along with the viral and cellular membranes in which they reside.[13,14] This close membrane apposition combined with lipid bilayer destabilization produced by membrane insertion of the FP leads to fusion.

Isolated FPs have been very useful in elucidating the mechanisms of viral fusion because (i) they can induce fusion by themselves and (ii) single mutations within FPs can lead to

Received: May 23, 2023
Accepted: July 17, 2023
Published: August 28, 2023

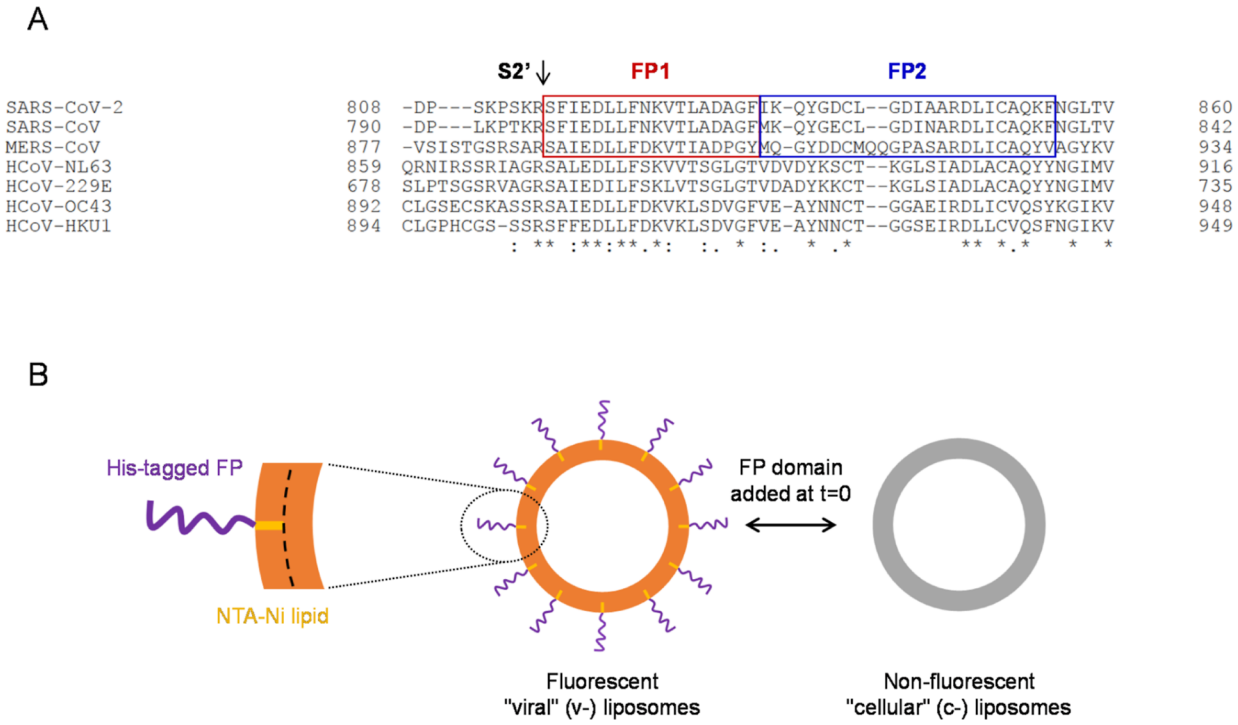

Figure 1. (A) Sequence alignment of Spike proteins from all human coronaviruses in the region immediately following the S2′ cleavage site known to be critical for SARS-CoV-2 fusion. The alignment was performed with the Clustal Omega program using the following sequences obtained from UniProt: SARS-CoV2 (P0DTC2), SARS-CoV (P59594), MERS-CoV (K9N5Q8), HCoV-NL63 (Q6Q1S2), HCoV-229E (P15423), HCoV-OC43 (P36334), and HCoV-HKU1 (Q5MQD0). The fusion peptides FP1 (red) and FP2 (blue) are highly conserved notably among MERS-CoV, SARS-CoV, and SARS-CoV-2. (B) Experimental setup used to study the capacity of SARS-CoV-2 fusion peptides to mediate membrane fusion *in vitro*. Fusion peptides with a C-terminal His_6 tag were reconstituted at $t = 0$ of the assay into fluorescently labeled liposomes mimicking the viral envelope (v-liposomes) by binding to lipids having an NTA-Ni headgroup. Fusion was monitored between v-liposomes and unlabeled peptide-free liposomes mimicking the cellular membrane (c-liposomes) using a FRET-based lipid mixing assay.

complete loss of viral fusion and infection.[15,16] FPs usually consist of about 20 amino acids, mostly hydrophobic, and are highly conserved within a given viral family.[15,17] Contrary to other type I viral fusion proteins, such as those of HIV and influenza viruses, which possess a single FP, several potential FPs with membrane interaction and/or membrane fusion activity were identified within the S2 subunit of S proteins of coronaviruses.[18] The region FP1 (residues 816−833 in SARS-CoV-2) is however believed to be the functional FP based on its high sequence conservation (particularly among MERS-CoV, SARS-CoV, and SARS-CoV-2) and its location immediately downstream of the S2′ cleavage site that is known to be critical for fusion of coronaviruses[6,15,19,20] (Figure 1A). In the case of SARS-CoV, FP1 was shown to induce membrane fusion, and some mutations that abolished the FP1-mediated liposome fusion *in vitro* also affected cell−cell fusion and viral infection *in situ*.[15] The region just C-terminal of FP1 (residues 834−855 in SARS-CoV-2, called FP2) was proposed to complement FP1 to form an extended fusion peptide (FP1−FP2) with higher membrane affinity.[21] Recent experimental and computational structural studies showed that the FP1 of SARS-CoV-2 inserts deeply into lipid bilayer structures, whereas its FP2 stays around the bilayer surface,[22−27] suggesting strong membrane perturbing effect and thus fusion activity by FP1.

The activity of viral FPs also depends on the lipid composition of the fusing membranes.[28] The FP of SARS-CoV was found to bind stronger and to penetrate deeper into membranes containing cholesterol (CHOL).[29] Interestingly, a recent study showed that the enzyme CHOL 25-hydroxylase could inhibit infection by MERS-CoV, SARS-CoV, and SARS-CoV-2 by inducing depletion of plasma membrane CHOL, thus blocking viral fusion at the cell surface.[30] Along the same lines, generation of ceramide (CER) membrane domains at the cell surface upon cleavage of sphingomyelin by the acid sphingomyelinase was found to facilitate SARS-CoV-2 entry into cells.[31] This suggests that repurposing drugs which can modify the structure or lipid composition of the host cell membrane could be an effective treatment against SARS-CoV-2 infection. In this regard, antipsychotic (AP) drugs are interesting candidates that were proposed to exert some antiviral activity against coronaviruses.[32−34] Because of their amphiphilic property and planar geometry, AP drugs are known to intercalate into lipid bilayers and thus modify their biophysical properties,[35] which can in turn impact the ability of these lipid bilayers to fuse.

In this paper, we have investigated *in vitro* with a fluorescence resonance energy transfer (FRET)-based liposome fusion assay the capacity of FP1 and FP2 from SARS-CoV-2 S protein to fuse the membranes of various lipid compositions (including or not CHOL and CER). We have also tested the ability of the AP chlorpromazine (CPZ) to inhibit FP-mediated membrane fusion. The effect of lipid composition and CPZ addition was also examined *in situ* on full-length S protein-mediated membrane fusion measured by a nanoluciferase-based cell fusion assay.

https://doi.org/10.1021/acsomega.3c03610
ACS Omega 2023, 8, 32729−32739

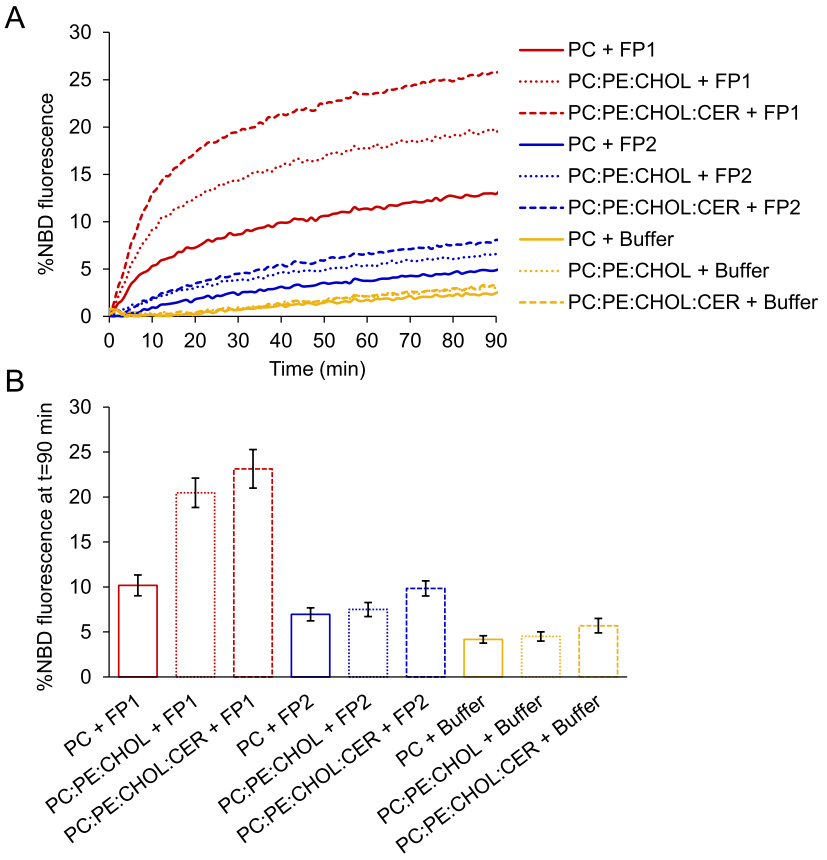

Figure 2. (A) Representative FRET-based lipid mixing experiments between v-liposomes (composed of 92 mol % PC, 5 mol % NTA-Ni, 1.5 mol % NBD, and 1.5 mol % Rho) and c-liposomes of various lipid compositions (including or not 10 mol % PE and 30 mol % CHOL or 10 mol % PE, 30 mol % CHOL, and 20 mol % CER at the expense of PC) in the absence (yellow) or presence of FP1 (red) or FP2 (blue) added at $t = 0$ (500 μM lipids and 25 μM peptides). FP1 induced efficient lipid mixing between v- and c-liposomes exclusively composed of PC lipid. Fusion was strongly activated when the c-liposome membrane contained PE and CHOL or PE, CHOL, and CER. No significant lipid mixing was measured under the same conditions with the FP2 peptide, or when the fusion peptides were not lipid-anchored (v-liposomes devoid of NTA-Ni lipids; see Figure S1). (B) Average extent of lipid mixing after 90 min (n = 4−9 independent experiments; error bars are standard errors).

RESULTS

The fusion activity of FP1 and FP2 from the SARS-CoV-2 S protein was examined *in vitro* through their capacity to mediate the fusion between two liposome populations, mimicking viral and cellular membranes, respectively. We used synthetic peptides with a C-terminal His_6 tag allowing their chemical coupling to reactive DOGS NTA (nickel salt) (NTA-Ni lipids) included in the liposome membrane (Figure 1B). Similar lipid-anchorage strategy has proven successful in recapitulating soluble N-ethylmaleimide-sensitive factor attachment protein receptor (SNARE)-mediated membrane fusion *in vitro*[36] and more recently in revealing the role of the heptad repeat domains of Mitofusin in mitochondrial membrane docking and fusion.[37] Fusion was measured using a FRET-based lipid mixing assay.[38] One population of liposomes (the fluorescent donor liposomes mimicking viral membranes, v-liposomes) had NTA-Ni lipids in their bilayer, whereas the other population (the non-fluorescent acceptor liposomes mimicking cellular membranes, c-liposomes) did not have any NTA-Ni lipid (Figure 1B). FP1 and FP2 were thus able to anchor exclusively onto the v-liposome surface. This allowed us to mimic the asymmetry that occurs during viral infection, where the fusogen is anchored onto the viral membrane and fuses with the cell membrane that lacks the fusogen. FP1 and FP2 were added at $t = 0$ of the lipid mixing assay, and their capacity to mediate fusion between the v- and c-liposomes was monitored for 90 min.

We started with v- and c-liposomes composed exclusively of phosphatidylcholine (PC), one of the main lipids of biological membranes. FP1 induced robust fusion between PC v- and c-liposomes, whereas no significant fusion was observed with FP2 under the same experimental conditions (Figure 2). In addition, no fusion was measured when FP1 was added to the v-liposomes lacking NTA-Ni lipids (Figure S1), indicating that FP1 needed to be membrane-anchored to induce lipid mixing in our system.

To study the effect of cellular membrane lipid composition on FP1-mediated fusion, we measured the fusion between v-liposomes composed exclusively of PC lipids and c-liposomes, including (in addition to PC) CHOL and CER lipids that were recently proposed to facilitate SARS-CoV-2 infection.[30,31] We also added phosphatidylethanolamine (PE) in the c-liposome membrane to better mimic the lipid composition of the outer leaflet of mammalian plasma membranes.[39] Having PE and CHOL together in the c-liposome membrane dramatically increased FP1-mediated fusion (Figures 2 and 3), whereas addition of either PE or CHOL alone had no significant effect on fusion (Figure S2). Including CER in the c-liposome membrane (in addition to PC, PE, and CHOL) further increased fusion mediated by FP1 (Figures 2 and 3). For all lipid compositions tested, FP1 needed to be anchored to the v-

https://doi.org/10.1021/acsomega.3c03610
ACS Omega 2023, 8, 32729−32739

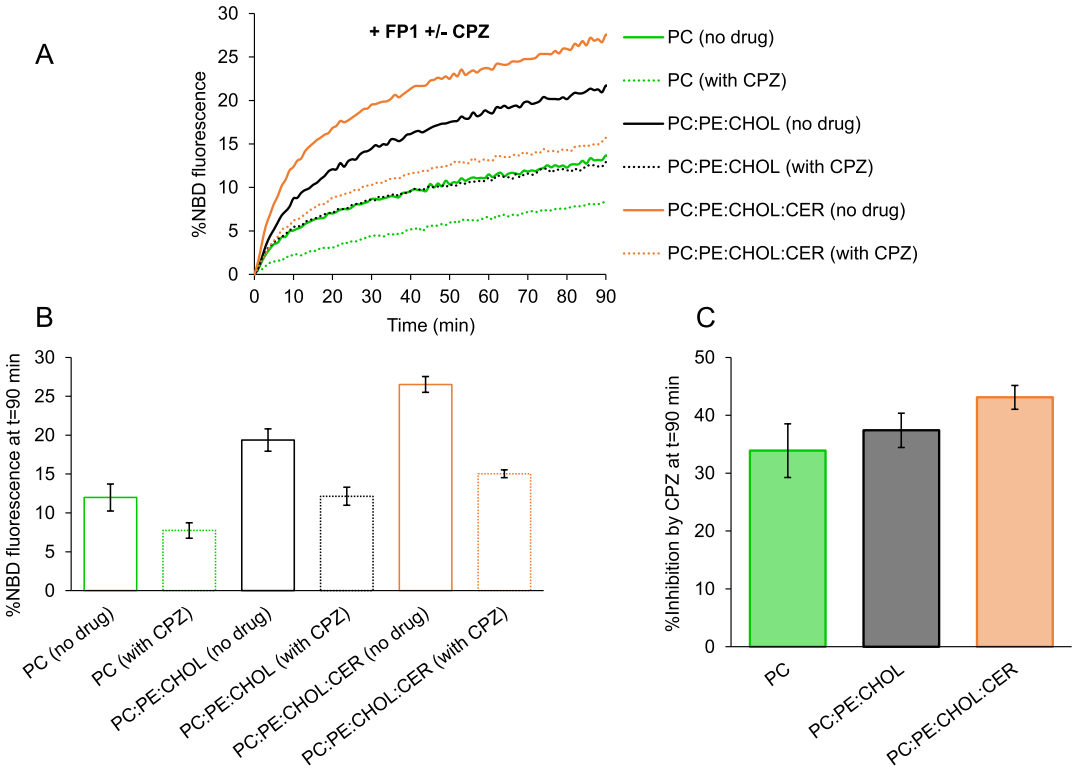

Figure 3. (A) Representative FRET-based lipid mixing experiments between v-liposomes (composed of 92 mol % PC, 5 mol % NTA-Ni, 1.5 mol % NBD, and 1.5 mol % Rho) and c-liposomes of various lipid compositions (including or not 10 mol % PE and 30 mol % CHOL or 10 mol % PE, 30 mol % CHOL, and 20 mol % CER at the expense of PC) in the presence of FP1 and in the presence/absence of CPZ, both added at $t = 0$ (500 μM lipids, 25 μM peptides, and 50 μM CPZ). All fusion experiments (with or without CPZ) were performed with a final DMSO concentration of 1% (v/v) in buffer H. CPZ strongly inhibited FP1-mediated fusion between v- and c-liposomes regardless of the c-liposome membrane lipid composition. (B) Average extent of lipid mixing after 90 min ($n = 4–6$ independent experiments; error bars are standard errors). (C) Percentage of fusion inhibition by CPZ after 90 min.

liposome membrane to induce fusion with c-liposomes (Figure S1).

Fusion mediated by FP2 slightly increased upon modification of the c-liposome membrane lipid composition but remained low and close to the fusion background observed in the absence of any fusion peptide (Figures 2 and S2). Of note, having PE in the c-liposome membrane activated all fusion events by 10−20%, whether induced by fusion peptides or not. This agrees well with the known role of PE lipids as facilitators of membrane fusion.[40]

Because high membrane curvature is known to activate fusion,[41−43] we analyzed the size of c-liposomes as a function of their lipid composition by multi-angle dynamic light scattering (MADLS). We found that the size distribution of c-liposomes was not significantly affected by their lipid composition (Figure S3). Importantly, the c-liposomes exclusively composed of PC lipid were overall smaller than the c-liposomes of more complex lipid compositions. Strong FP1-mediated membrane fusion measured in the presence of PE and CHOL or PE, CHOL, and CER is therefore not due to the high membrane curvature of c-liposomes.

Next, we tested the effect of the AP drug CPZ on FP1-mediated membrane fusion. CPZ is known as an antagonist of several G-protein-coupled receptors, including dopamine receptors,[44] but it is also known for its capacity to bind and perturb the membrane structure.[35,45,46] CPZ was solubilized in dimethyl sulfoxide (DMSO) and added at the very beginning of the lipid mixing assay, together with the fusion peptide. The final DMSO concentration was 1% (v/v) to ensure that it would not affect the biophysical properties of liposome membranes.[47] CPZ inhibited FP1-mediated fusion between v- and c-liposomes and induced a similar decrease of about 40% of the extent of fusion for all lipid compositions tested (Figure 3). To check if this observation was specific to CPZ, we also examined the effect of the antidepressant (AD) drug Fluvoxamine (FLUV), which also has amphiphilic and membrane-binding properties.[48] Under the same experimental conditions, FLUV only had a modest inhibitory effect on FP1-mediated fusion (Figure S4).

The extended fusion peptide composed of FP1 and FP2 (FP1−FP2) was previously shown to exhibit greater membrane activity than FP1 or FP2 alone.[21] We thus wanted to check if this translated into a greater ability of FP1−FP2 to induce membrane fusion. We chose to work with c-liposomes composed of PC, PE, and CHOL, corresponding to the simplest lipid composition that activated fusion by FP1. FP1−FP2 triggered efficient fusion between v- and c-liposomes, and the extent of lipid mixing at the end of the reaction (about 20%) was similar to that measured with FP1 (Figures 3 and S5). The drugs CPZ and FLUV also had the same effect on FP1- or FP1−FP2-induced membrane fusion. CPZ decreased fusion between v- and c-liposomes by about 30% and FLUV did not have any significant effect on fusion (Figure S5). In our system, FP1 and FP1−FP2 thus displayed the same fusion activity and responded similarly to the addition of the AP drug CPZ or the AD drug FLUV.

To confirm the biological relevance of our *in vitro* data, we used a cell-based assay, in which we could test the impact of

https://doi.org/10.1021/acsomega.3c03610
ACS Omega 2023, 8, 32729−32739

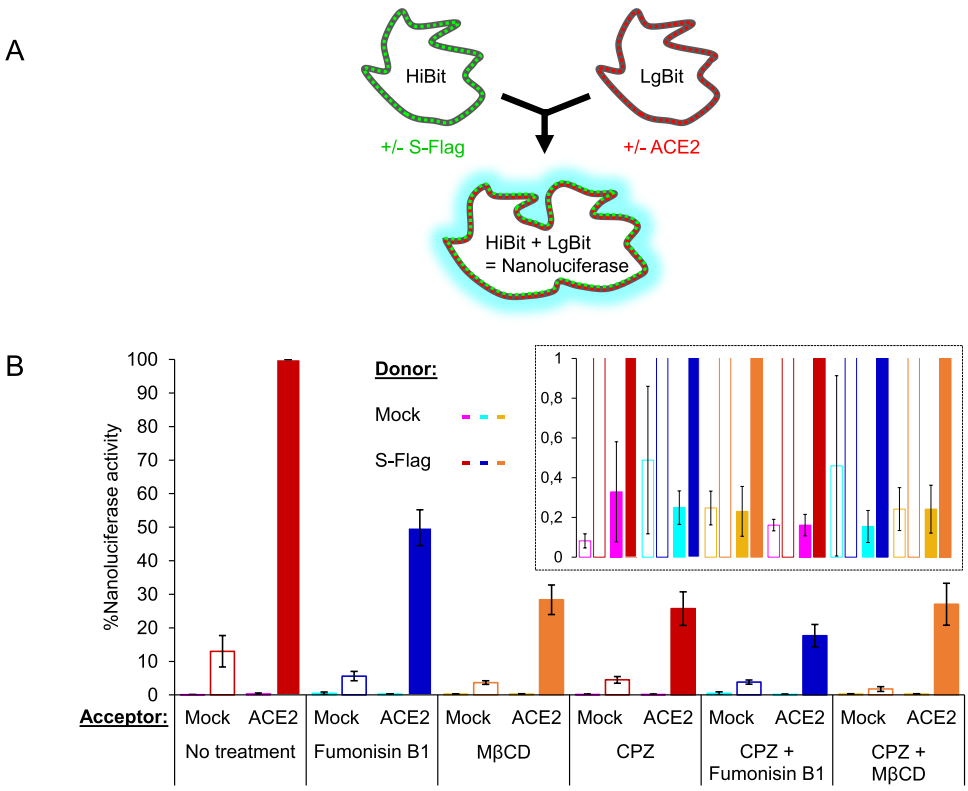

Figure 4. Effect of drugs on *in situ* cell−cell fusion. (A) Assay principle: HeLa cells stably expressing HiBit-Hsp70 and either co-expressing C-terminally Flag-tagged wild-type Spike (S-Flag) or not were co-cultured with HeLa cells stably expressing LgBit and either co-expressing ACE2 or not. Cell−cell fusion triggers content mixing and nanoluciferase complementation. (B) Donor cells (HiBit-Hsp70 positive cells) either co-expressing S-Flag or not (mock) were co-cultured with acceptor cells (LgBit positive cells) either co-expressing ACE2 or not (mock). After 24 h, Fumonisin B1 (20 μM) or MβCD (2 mM) and/or CPZ (10 μM) were added for 24 h prior to reading nanoluciferase activity. The graph represents the percentage of nanoluciferase activity for each condition. Nanoluciferase activity resulting from content mixing between donor cells co-expressing S-Flag and acceptor cells co-expressing ACE2 was set to 100%. The inset shows the background nanoluciferase activity measured when the donor cells do not co-express S-Flag (n = 2 independent experiments in triplicates; error bars represent standard deviations of all replicates).

drugs that are known to modify CHOL and CER levels in the cell plasma membrane.[49,50] We performed *in situ* measurement of cell−cell fusion between (i) donor HeLa cells that stably expressed the first half of a split nanoluciferase (HiBit-Hsp70) in their cytosol with or without Flag-tagged S proteins on their surface and (ii) acceptor HeLa cells that stably expressed the second half of the split nanoluciferase (LgBit) in their cytosol with or without ACE2 receptors on their surface. Split nanoluciferase complementation occurs only in case of cell−cell fusion (Figure 4A). We incubated donor and acceptor cells in the presence or absence of S proteins and ACE2 receptors to establish that both proteins were required for efficient fusion. We observed that luminescence activity was well above the background signal only when S and ACE2 were present on donor and acceptor cells, respectively (Figure 4B). This value was set to 100%. Note that in the absence of overexpressed ACE2 on acceptor cells, the luminescence activity was about 15%. This is consistent with the very low endogenous level of ACE2 on HeLa cells, which was shown to be below that required for SARS-CoV-2 infection but not so low as to prevent S-mediated cell−cell fusion.[8,51] We then performed the same experiments in the presence of Fumonisin B1, a well-known inhibitor of CER synthase that dramatically reduces the level of CER.[50] This led to a 50% decrease of the fusion signal (Figure 4B). When we added MβCD to artificially deplete the plasma membrane of CHOL, this also led to a strong (70%) inhibition of cell−cell fusion. Interestingly, CPZ treatment showed a similar effect on cell−cell fusion (70% inhibition) as removing CHOL, and we could not detect any additive effect when CPZ was added together with MβCD. Note that the donor and acceptor cells were incubated together for at least 16 h to allow them to adhere before the drugs were added, which may have caused occasional cell−cell fusion. In addition, our assay required the use of long-term (24 h) drug treatment, which is unusual, especially for mβCD. Importantly, we ensured that the drug treatment did not induce any cell death or growth (Figure S6). Nevertheless, the cell−cell fusion assay confirms the *in vitro* results and shows that CHOL and CER depletion, and CPZ addition, inhibit S-mediated membrane fusion.

DISCUSSION

Our study shows that the fusion peptide FP1 of the S protein from SARS-CoV-2 mediates the fusion between liposomes to which it is membrane-anchored (v-liposomes mimicking the viral envelope) and protein-free liposomes (c-liposomes mimicking the cellular plasma membrane). On the contrary, the fusion peptide FP2 could not induce fusion between v- and c-liposomes in our system (Figures 2 and S2). This agrees with a recent structural study which found that FP1 becomes more structured in contact with lipid bilayers and inserts below the lipid headgroups, while FP2 remains unstructured and lies on

https://doi.org/10.1021/acsomega.3c03610
ACS Omega 2023, 8, 32729−32739

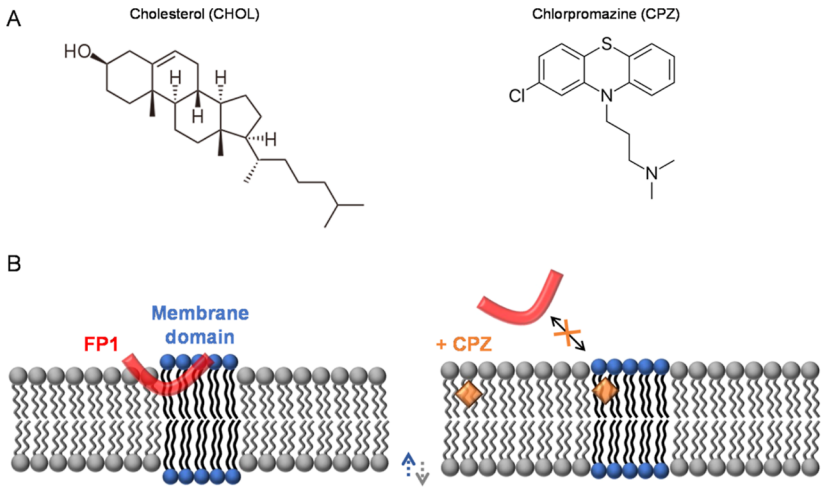

Figure 5. (A) Structure of CHOL and CPZ. Both molecules are amphipathic and display a ring-like planar structure. (B) Proposed mechanism of action for FP1 on the cellular membrane. FP1 may interact with the boundaries of membrane domains (depicted in blue) that contain CHOL or CER molecules (not shown here for clarity). CPZ may inhibit FP1−membrane interaction and FP1-induced fusion by altering lipid order, specifically increasing the bilayer thickness outside of membrane domains while decreasing it within these domains.

the surface of the lipid bilayers. It was then proposed that deeper membrane insertion in the case of FP1 should induce stronger perturbing effects on the lipid bilayer structure and thus favor fusion.[22] Recent work employing neutron scattering techniques found that FP1 could in fact disrupt membranes and induce an increase in lipid tail dynamics, which is consistent with the weakening of membrane structural integrity.[26]

Experiments using electron spin resonance spectroscopy on FP1 and FP2 from SARS-CoV-2 found that FP1 and FP2 can cooperate and penetrate deeper into the lipid bilayer structure when they are together.[21] In our liposome fusion assay, FP1−FP2 displayed the same fusion activity as FP1 (Figures 3 and S5). The synergy between FP1 and FP2 was thus not observed in our experiments with FP1 and FP2 from SARS-CoV-2 or at least it did not translate into stronger fusion activity.

Previous studies have observed lipid mixing with fusion peptides that were not lipid-anchored and have highlighted the influence of pH on fusion activity. A recent study by Birtles *et al.*[52] demonstrated that the fusion peptide FP1−FP2 of SARS-CoV-2 induced greater lipid mixing at pH 5 compared to that at pH 7. This effect was attributed to the elongation of helix 1 of FP1 at pH 5, resulting in deeper embedding of FP1 into the membrane. Similarly, an earlier study by Madu *et al.*[15] also reported enhanced lipid mixing by the fusion peptide FP1 of SARS-CoV at lower pH levels.

We propose that the charge of the peptide also plays a role in this phenomenon. Madu *et al.*[15] used the fusion peptide FP1 of SARS-CoV (798-SFIEDLLFNKVTLADAGFMKQY-819) with a C-terminal GCGKKK linker. The isoelectric point (pI) of this peptide is 9.4, making it positively charged at pH 7 and lower. Birtles *et al.*[52] employed the fusion peptide FP1−FP2 of SARS-CoV-2 (816-SFIEDLLFNKVTLADAGFIK-QYGDCLGDIAARDLICAQKF-855) with an N-terminal His_6 tag. The pI of this peptide is 6.3, rendering it negatively charged at pH 7 and positively charged at pH 5.

Both studies conducted lipid mixing experiments using liposomes containing negatively charged phosphatidylserine or phosphatidylglycerol lipids. Consequently, fusion peptides may have interacted with the liposome membrane through electrostatic attraction, obviating the need for lipid anchoring them to induce fusion. These findings provide valuable insights into the pH-dependent lipid mixing activity of the fusion peptide, shedding light on the endosomal pathway of SARS-CoV-2 entry.[11,53]

The lipid composition of the membrane can also significantly impact fusion activity. In our experiments, we observed that adding PE and CHOL into the c-liposome membrane to better recapitulate the lipid composition of the outer leaflet of mammalian plasma membranes strongly enhanced FP1-induced fusion between v- and c-liposomes (Figures 2 and 3). In our cell−cell fusion assay, depletion of plasma membrane CHOL in the presence of MβCD induced a dramatic (∼70%) decrease of fusion between the cells expressing S proteins and the cells expressing ACE2 receptors (Figure 4). This agrees well with two recent studies which found that efficient SARS-CoV-2 fusion with the cell membrane requires CHOL,[30,54] and with the fact that several CHOL-recognition motifs have been identified in various regions of the S protein, including the FP1 domain.[55] Interestingly, the effect of CHOL on FP1-mediated liposome fusion was only observed when PE was also present in the membrane (Figures 2 and S2). This can be explained by the ability of PE to induce CHOL-enriched domains as seen on time-of-flight secondary ion mass spectrometry (TOF-SIMS) images of PC/PE/CHOL mixtures.[56] Such CHOL domains may facilitate FP1−membrane interaction and FP1-induced fusion, particularly at their boundaries[57] (Figure 5).

Cellular infection by SARS-CoV-2 was also previously found to be facilitated by the presence of CER in the cell plasma membrane.[31] CER molecules are known to assemble into large hydrophobic gel-like domains in the outer leaflet of the cell plasma membrane that can serve to sequester specific surface proteins. It was proposed that such CER-enriched domains could trap ACE2 and TMPRSS2 to facilitate S protein binding and priming, respectively.[58] We hypothesized that CER-enriched domains, because of their high hydrophobicity, could also favor FP1 interaction with the cell membrane and thus membrane fusion. Addition of CER into the c-liposome membrane in fact increased FP1-mediated fusion between v- and c-liposomes *in vitro* (Figures 2 and 3), and depletion of CER upon treatment of cells with Fumonisin B1 decreased S-

https://doi.org/10.1021/acsomega.3c03610
ACS Omega 2023, 8, 32729−32739

mediated cell−cell fusion *in situ* (Figure 4). CER could thus promote SARS-CoV-2 infection in two distinct ways: (i) by facilitating S protein binding/priming and (ii) by directly activating the fusion step.

The observation that CHOL and CER facilitate S-mediated membrane fusion prompted us to investigate the effect of the approved drugs that can modify membrane lipid composition and/or structure and could thus be repurposed to inhibit SARS-CoV-2 infection. We focused on the AP drug CPZ because of its previously proposed antiviral activity and its known effects on membrane's biophysical properties. Several recent studies revealed that AP drugs could be effective in reducing SARS-CoV-2 infectivity. A screening assay based on morphological profiling of cells infected by SARS-CoV-2 identified two APs, domperidone and metoclopramide, exhibiting antiviral effects.[32] Another study searching for drugs targeting SARS-CoV-2 protein's interactome found that the AP drug haloperidol (HAL) displayed some antiviral activity.[33] Finally, CPZ was found to inhibit the replication of MERS-CoV, SARS-CoV, and SARS-CoV-2 in cultured cells.[34,59,60] It was furthermore suggested that CPZ might block viral replication at an early entry stage, which could be the fusion step.

In our study, addition of CPZ reduces FP1-mediated fusion *in vitro* and S-mediated fusion *in situ* (Figures 3 and 4). Interestingly, our *in vitro* and *in situ* fusion data also show that adding CPZ produces the same effect on fusion as depleting the membrane of CHOL (Figures 2−4). CPZ was previously found to modify the lateral organization of CHOL-containing membranes and to perturb raft domains, specifically decreasing lipid order in membrane regions enriched with CHOL. This effect can be attributed to the ability of CPZ to compete with CHOL as CPZ and CHOL share a similar ring-like planar structure[35,45] (Figure 5). It is tempting to speculate that such competition between CPZ and CHOL could explain the inhibitory effect of CPZ on the S-mediated membrane fusion observed in our study. This would also explain why CPZ had no effect on S-mediated cell−cell fusion when cells were treated with MβCD. *In vitro*, however, the inhibitory effect of CPZ persisted regardless of the lipid composition of the liposomes. This could be because (i) CPZ was also shown to increase lipid order in membranes or membrane regions lacking CHOL[35,45] (Figure 5) and (ii) *in vitro* systems, which are intrinsically simpler in terms of their lipid and protein composition, are more sensitive to perturbations of the membrane structure. Under the same experimental conditions, the AD drug FLUV, an amphiphilic ring-like molecule that also interacts with membranes but has little effect on their biophysical properties,[48] did not significantly alter FP1-mediated membrane fusion (Figure S4). The inhibitory effect of CPZ on FP1-induced fusion could therefore result from its ability to increase lipid order and thus counterbalance the perturbing effect of FP1 on the membrane structure (Figure 5).

So far, therapeutic strategies targeting the S2 fusion machinery mainly focused on the development of anti-fusogenic synthetic peptides, mimicking the HR2 domain. Such peptides were shown to inhibit formation of the native HR1/HR2 six-helix coiled-coil hairpin complex, thus preventing viral fusion and infection by several human coronaviruses *in situ*, including MERS-CoV, SARS-CoV, and SARS-CoV-2.[61−63] Furthermore, intranasal injection of a synthetic lipopeptide derived from HR2 was found to protect ferrets against infection by SARS-CoV-2.[64] These promising effects of anti-fusogenic synthetic HR2 peptides remain however to be evaluated in the context of human clinical trials. To circumvent the complex processes associated with the development of new drugs, an alternative strategy consists in repositioning existing approved drugs by testing their capacity to block SARS-CoV-2 fusion with target cells. Our study is in line with this approach and suggests that amphiphilic molecules with a planar shape such as CPZ could be effective inhibitors of SARS-CoV-2 infection due to their ability to modify the structure of membranes.

MATERIALS AND METHODS

Chemicals. 1-Palmitoyl-2-oleoyl-*sn*-glycero-3-phosphocholine (PC), 1,2-dioleoyl-*sn*-glycero-3-phosphoethanolamine (PE), 1,2-dioleoyl-*sn*-glycero-3-phospho-L-serine-*N*-(7-nitro-2-1,3-benzoxadiazol-4-yl) (ammonium salt) (NBD), 1,2-dioleoyl-*sn*-glycero-3-phosphoethanolamine-*N*-(lissamine rhodamine B sulfonyl) (ammonium salt) (Rho), and 1,2-dioleoyl-*sn*-glycero-3-[(*N*-(5-amino-1-carboxypentyl)iminodiacetic acid)-succinyl] (nickel salt) (NTA-Ni) were purchased from Avanti Polar Lipids as chloroform solutions. CHOL and *N*-stearoyl-D-*erythro*-sphingosine (CER) were purchased from Avanti Polar Lipids as powder and solubilized in analytical grade chloroform.

N-2-Hydroxyethylpiperazine-*N*′-2-ethanesulfonic acid (HEPES, OmniPur grade), potassium hydroxide solution 47% (KOH 47%, EMSURE grade for analysis), potassium chloride (KCl, OmniPur grade), glycerol (Molecular Biology grade), n-octyl-β-D-glucopyranoside (β-OG, ≥98% GC), *n*-dodecyl β-D-maltoside (DDM, ULTROL grade), DMSO (Molecular Biology grade), chlorpromazine hydrochloride (CPZ, ≥98% TLC), and fluvoxamine maleate (FLUV, ≥97% HPLC) were purchased from Merck.

All aqueous solutions were prepared using 18.2 MΩ ultrapure water and filtered with sterile 0.22 μm polyethersulfone (PES) membranes.

Peptides. Fusion peptide domains (FP1, FP2, and FP1−FP2) of the SARS-CoV-2 spike protein were synthesized by GenScript with a purity ≥95%. The produced sequences were FP1 (816-SFIEDLLFNKVTLADAGF-833), FP2 (834-IKQYGDCLGDIAARDLICAQKF-855), and FP1−FP2 (816-SFIEDLLFNKVTLADAGFIKQYGDCLGDIAARDLICAQKF-855); the three constructs included a C-terminal Leu-His_6 tag. Lyophilized samples (1 mg aliquots) were solubilized in 1 mL of buffer H (25 mM HEPES/KOH, pH 7.5; 150 mM KCl; 10% (v/v) glycerol) by vortexing for 2 min at room temperature. Samples were snap-frozen in liquid nitrogen and stored at −80 °C as aliquots of 50 μL.

Liposomes. Liposomes were generated by the detergent-assisted method.[38] 0.9 μmol of the appropriate lipid mixtures in chloroform was dried in glass tubes for 10 min under a gentle stream of argon, followed by 2 h under vacuum. The dried lipid films were resuspended in 300 μL of buffer H containing 1% (w/v) β-OG by vigorously vortexing for 30 min at room temperature or 50 °C when CER was included in the lipid mixture. The detergent concentration was next reduced below the critical micellar concentration, 0.33% (w/v), by slowly adding 600 μL of buffer H, and then the detergent was removed by overnight flow dialysis at 4 mL/min against 4 L of buffer H. Liposomes (final lipid concentration of 1 mM) were stored on ice and protected from light for up to 2−3 weeks.

https://doi.org/10.1021/acsomega.3c03610
ACS Omega 2023, 8, 32729−32739

FRET-Based Lipid Mixing Assay. 27 μL of acceptor (non-fluorescent) liposomes at 1 mM and 21 μL of buffer H [or 15 μL of buffer H and 6 μL of drugs at 500 μM in DMSO 10% (v/v) in buffer H for experiments performed in the presence of drugs] were added to a flat bottom 96-well white polystyrene plate (Thermo Scientific) and pre-warmed at 37 °C for 7 min; 6 μL of donor (fluorescent) liposomes at 500 μM was carefully added to one side of the well; 6 μL of peptides at 250 μM in buffer H was added to another side of the well. The fusion reaction was initiated by shaking the plate in order to mix the three different solutions. Lipid mixing was measured by following fluorescence dequenching of the NBD probes from the donor liposomes resulting from their dilution into the acceptor liposomes. The NBD fluorescence was monitored at 1 min intervals for 90 min (excitation at 460 nm; emission at 535 nm; and cutoff at 530 nm) by the SpectraMax M5 microplate reader (Molecular Devices) equilibrated to 37 °C. After 90 min, 10 μL of 2.5% (w/v) DDM was added to completely dissolve the liposomes and thus measure the NBD fluorescence at infinite dilution, F_{max}(NBD); the data were then normalized using the following equation that gives the percentage of NBD fluorescence increase at time t, % F(NBD, t)

$$\%\,F(\mathrm{NBD}, t) = [F(\mathrm{NBD}, t) - F_{min}(\mathrm{NBD})] / [F_{max}(\mathrm{NBD}) - F_{min}(\mathrm{NBD})]$$

where F_{min}(NBD) is the lowest NBD fluorescence value from all time points.

Multi-Angle Dynamic Light Scattering. 10 μL of liposomes at 1 mM and 90 μL of buffer H were mixed in a low volume quartz batch cuvette (ZEN2112, Malvern Panalytical), and their size distribution was determined at 37 °C with the Zetasizer Ultra Red instrument (Malvern Panalytical) using the MADLS mode, which measures the correlation function in three scattering directions: back scatter (173°), side scatter (90°), and forward scatter (13°).

Plasmids. The LgBit construct was obtained by removing the EGFP-Hsp70 sequence from the pEGFP-Hsp70 plasmid (Addgene#15215), which was replaced by the PCR-amplified LgBit insert from LgBit Expression Vector (Promega#N2681). AgeI and SpeI restriction enzymes [New England Biolabs (NEB)] were used to digest both the plasmid and the insert before ligation using T4 DNA Ligase (NEB). Similarly, the HiBit-Hsp70 construct was obtained by removing the EGFP-Hsp70 sequence from the pEGFP-Hsp70 plasmid using AgeI and SpeI. The HiBit-Hsp70 insert was PCR-amplified directly from the pEGFP-Hsp70 plasmid using primers containing the HiBit sequence and then inserted using AgeI and XbaI (NEB), which is SpeI compatible. The primers used to amplify LgBit sequence were as follows: AgeI-LgBit forward 5′-TAG ACC GGT CAC CAT GGT CTT CAC ACT CGA AGA-3′ and SpeI-LgBit reverse 5′-TCC ACT AGT AAC GTT ACT CGG AAC AGC ATG GAG-3′. The primers used to amplify HiBit-Hsp70 sequence were as follows: AgeI-HiBit-Hsp70 forward 5′-GCC ACC GGT ACC ATG ACT AGT GTG AGC GGC TGG CGG CTG TTC AAG AAG ATT AGC GGA TCC TCC GGT GGA TCG AGC GGT GGG AAT TCT GGT GGA GGA TCC GCT AGC ATG GCC AAA GCC GCG-3′ and XbaI-Hsp70 reverse 5′-GCA TCT AGA AGA GCT CGT CTC AAG CTT GCT AAT CTA CCT CCT CAA TGG TGGG-3′.

The plasmid of wild-type spike with a C-terminal Flag tag was generated by the Biochemistry and Biophysics (B & B) facility of the Institute of Psychiatry and Neuroscience of Paris (IPNP). The vector pcDNA3.1(-) containing the SARS-CoV-2, Wuhan-Hu-1 Spike glycoprotein gene (pcDNA3.1-Spike-WT) was kindly provided by BEI resources (#NR-52420). The C-terminal Flag tag was introduced into pcDNA3.1-Spike-WT thanks to NEBuilder HiFi DNA Assembly (NEB). The Flag tag was added during the amplification of Spike-WT from pcDNA3.1-Spike-WT with the primers: forward 5′-ACC ACA AAG CGG ACA ATG TTC GTG TTT CTG GTG CTG-3′ and reverse 5′-ACC GAG CTC GGA TCC TCA TTT ATC ATC ATC ATC TTT ATA ATC GCT GCC GGT GTA GTG CAG CTT CACG-3′. The resulting plasmid called pcDNA3.1-Spike-WT-Flag was amplified and verified by sequencing.

The human ACE2 plasmid was purchased from VectorBuilder (#VB900122-0052prs).

Cell Culture. HeLa cells (ATCC) were cultured in DMEM (Gibco) complemented with 10% FBS (Gibco or Biosera) at 37 °C and 5% CO_2. Stable cell lines were selected with Geneticin 10 μg/mL (Gibco) after Lipofectamine 2000-based transfection (Invitrogen).

Cell−Cell Fusion Assay. 100,000 donor cells (HiBit-Hsp70) were transfected with or without Spike-WT-Flag encoding plasmid (1 μg of DNA/1 μL of Lipofectamine 2000) in a 24-well plate format. Similarly, 100,000 acceptor cells (LgBit) were transfected with or without ACE2 encoding plasmid (1 μg of DNA/1 μL of Lipofectamine 2000). When required, donor and acceptor cells were only treated with Lipofectamine 2000 (mock). At 8 h post-transfection, the cells were washed three times with phosphate-buffered saline, trypsinized, and resuspended in complete media. 20,000 cells (for each donor and/or acceptor cells) were seeded in a white 96-well plate format and cultured for 24 h. When required, Fumonisin B1 (20 μM) or MβCD (2 mM) and/or CPZ (10 μM) was added for 24 h prior to reading nanoluciferase activity using the Nano-Glo Live Cell Assay System (Promega) and SpectraMax iD3 microplate reader (Molecular Devices).

■ ASSOCIATED CONTENT

Supporting Information

The Supporting Information is available free of charge at https://pubs.acs.org/doi/10.1021/acsomega.3c03610.

> Liposome fusion experiments featuring non-lipid-anchored fusion peptides, effect of PE or CHOL on fusion peptide-induced liposome fusion, liposome size distribution as a function of their lipid composition, effect of FLUV on FP1-mediated liposome fusion, effect of CPZ or FLUV on FP1-FP2-induced liposome fusion, and effect of Fumonisin B1, MβCD, and/or CPZ on cell viability (PDF)

■ AUTHOR INFORMATION

Corresponding Author

David Tareste − *Université Paris Cité, Inserm UMR-S 1266, Institute of Psychiatry and Neuroscience of Paris (IPNP), Paris 75014, France;* orcid.org/0000-0002-8744-7598; Email: david.tareste@inserm.fr

Authors

Kristina Niort − *Université Paris Cité, Inserm UMR-S 1266, Institute of Psychiatry and Neuroscience of Paris (IPNP), Paris 75014, France*

https://doi.org/10.1021/acsomega.3c03610
ACS Omega 2023, 8, 32729−32739

Julia Dancourt − *Université Paris Cité, Inserm U 1316, CNRS UMR 7057, Laboratoire Matières et Systèmes Complexes (MSC), Paris 75006, France*

Erwan Boedec − *Université Paris Cité, Inserm UMR-S 1266, Institute of Psychiatry and Neuroscience of Paris (IPNP), Paris 75014, France*

Zahra Al Amir Dache − *Université Paris Cité, Inserm U 1316, CNRS UMR 7057, Laboratoire Matières et Systèmes Complexes (MSC), Paris 75006, France*

Grégory Lavieu − *Université Paris Cité, Inserm U 1316, CNRS UMR 7057, Laboratoire Matières et Systèmes Complexes (MSC), Paris 75006, France;* orcid.org/0000-0001-9852-4977

Complete contact information is available at: https://pubs.acs.org/10.1021/acsomega.3c03610

Notes

The authors declare no competing financial interest.

■ ACKNOWLEDGMENTS

D.T. was funded by the "Agence Nationale de la Recherche" (ANR-19-CE11-0018-01), the "Fondation de France—Recherche fondamentale et clinique sur les maladies psychiatriques", and the "Association Française contre les Myopathies" (AFM-Téléthon Research grant 23778). Work in G.L laboratory was supported by INSERM, "Agence Nationale de la Recherche" (Excelldisc, BIOEV, EVfusion) and Chaire d'Excellence Idex, Université Paris Cité. Z.E.A.D. received a postdoctoral fellowship from "Fondation pour la Recherche Medicale" (FRM).

■ REFERENCES

(1) Matsuyama, S.; Ujike, M.; Morikawa, S.; Tashiro, M.; Taguchi, F. Protease-Mediated Enhancement of Severe Acute Respiratory Syndrome Coronavirus Infection. *Proc. Natl. Acad. Sci. U.S.A.* **2005**, *102*, 12543−12547.

(2) Shulla, A.; Heald-Sargent, T.; Subramanya, G.; Zhao, J.; Perlman, S.; Gallagher, T. A Transmembrane Serine Protease Is Linked to the Severe Acute Respiratory Syndrome Coronavirus Receptor and Activates Virus Entry. *J. Virol.* **2011**, *85*, 873−882.

(3) Park, J.-E.; Li, K.; Barlan, A.; Fehr, A. R.; Perlman, S.; McCray, P. B.; Gallagher, T. Proteolytic Processing of Middle East Respiratory Syndrome Coronavirus Spikes Expands Virus Tropism. *Proc. Natl. Acad. Sci. U.S.A.* **2016**, *113*, 12262−12267.

(4) Kawase, M.; Shirato, K.; van der Hoek, L.; Taguchi, F.; Matsuyama, S. Simultaneous Treatment of Human Bronchial Epithelial Cells with Serine and Cysteine Protease Inhibitors Prevents Severe Acute Respiratory Syndrome Coronavirus Entry. *J. Virol.* **2012**, *86*, 6537−6545.

(5) Shirato, K.; Kawase, M.; Matsuyama, S. Middle East Respiratory Syndrome Coronavirus Infection Mediated by the Transmembrane Serine Protease TMPRSS2. *J. Virol.* **2013**, *87*, 12552−12561.

(6) Hoffmann, M.; Kleine-Weber, H.; Schroeder, S.; Krüger, N.; Herrler, T.; Erichsen, S.; Schiergens, T. S.; Herrler, G.; Wu, N.-H.; Nitsche, A.; Müller, M. A.; Drosten, C.; Pöhlmann, S. SARS-CoV-2 Cell Entry Depends on ACE2 and TMPRSS2 and Is Blocked by a Clinically Proven Protease Inhibitor. *Cell* **2020**, *181*, 271−280.e8.

(7) Tang, T.; Bidon, M.; Jaimes, J. A.; Whittaker, G. R.; Daniel, S. Coronavirus Membrane Fusion Mechanism Offers a Potential Target for Antiviral Development. *Antiviral Res.* **2020**, *178*, 104792.

(8) Zhou, P.; Yang, X.-L.; Wang, X.-G.; Hu, B.; Zhang, L.; Zhang, W.; Si, H.-R.; Zhu, Y.; Li, B.; Huang, C.-L.; Chen, H.-D.; Chen, J.; Luo, Y.; Guo, H.; Jiang, R.-D.; Liu, M.-Q.; Chen, Y.; Shen, X.-R.; Wang, X.; Zheng, X.-S.; Zhao, K.; Chen, Q.-J.; Deng, F.; Liu, L.-L.; Yan, B.; Zhan, F.-X.; Wang, Y.-Y.; Xiao, G.-F.; Shi, Z.-L. A Pneumonia Outbreak Associated with a New Coronavirus of Probable Bat Origin. *Nature* **2020**, *579*, 270−273.

(9) Walls, A. C.; Park, Y.-J.; Tortorici, M. A.; Wall, A.; McGuire, A. T.; Veesler, D. Structure, Function, and Antigenicity of the SARS-CoV-2 Spike Glycoprotein. *Cell* **2020**, *181*, 281−292.e6.

(10) Wrapp, D.; Wang, N.; Corbett, K. S.; Goldsmith, J. A.; Hsieh, C.-L.; Abiona, O.; Graham, B. S.; McLellan, J. S. Cryo-EM Structure of the 2019-NCoV Spike in the Prefusion Conformation. *Science* **2020**, *367*, 1260−1263.

(11) Jackson, C. B.; Farzan, M.; Chen, B.; Choe, H. Mechanisms of SARS-CoV-2 Entry into Cells. *Nat. Rev. Mol. Cell Biol.* **2021**, *23*, 3−20.

(12) Ou, X.; Liu, Y.; Lei, X.; Li, P.; Mi, D.; Ren, L.; Guo, L.; Guo, R.; Chen, T.; Hu, J.; Xiang, Z.; Mu, Z.; Chen, X.; Chen, J.; Hu, K.; Jin, Q.; Wang, J.; Qian, Z. Characterization of Spike Glycoprotein of SARS-CoV-2 on Virus Entry and Its Immune Cross-Reactivity with SARS-CoV. *Nat. Commun.* **2020**, *11*, 1620.

(13) Walls, A. C.; Tortorici, M. A.; Snijder, J.; Xiong, X.; Bosch, B.-J.; Rey, F. A.; Veesler, D. Tectonic Conformational Changes of a Coronavirus Spike Glycoprotein Promote Membrane Fusion. *Proc. Natl. Acad. Sci. U.S.A.* **2017**, *114*, 11157−11162.

(14) Fan, X.; Cao, D.; Kong, L.; Zhang, X. Cryo-EM Analysis of the Post-Fusion Structure of the SARS-CoV Spike Glycoprotein. *Nat. Commun.* **2020**, *11*, 3618.

(15) Madu, I. G.; Roth, S. L.; Belouzard, S.; Whittaker, G. R. Characterization of a Highly Conserved Domain within the Severe Acute Respiratory Syndrome Coronavirus Spike Protein S2 Domain with Characteristics of a Viral Fusion Peptide. *J. Virol.* **2009**, *83*, 7411−7421.

(16) Alsaadi, E. A. J.; Neuman, B. W.; Jones, I. M. A Fusion Peptide in the Spike Protein of MERS Coronavirus. *Viruses* **2019**, *11*, 825.

(17) Walls, A. C.; Tortorici, M. A.; Bosch, B.-J.; Frenz, B.; Rottier, P. J. M.; DiMaio, F.; Rey, F. A.; Veesler, D. Cryo-Electron Microscopy Structure of a Coronavirus Spike Glycoprotein Trimer. *Nature* **2016**, *531*, 114−117.

(18) Millet, J. K.; Whittaker, G. R. Physiological and Molecular Triggers for SARS-CoV Membrane Fusion and Entry into Host Cells. *Virology* **2018**, *517*, 3−8.

(19) Belouzard, S.; Chu, V. C.; Whittaker, G. R. Activation of the SARS Coronavirus Spike Protein via Sequential Proteolytic Cleavage at Two Distinct Sites. *Proc. Natl. Acad. Sci. U.S.A.* **2009**, *106*, 5871−5876.

(20) Cai, Y.; Zhang, J.; Xiao, T.; Peng, H.; Sterling, S. M.; Walsh, R. M.; Rawson, S.; Rits-Volloch, S.; Chen, B. Distinct Conformational States of SARS-CoV-2 Spike Protein. *Science* **2020**, *369*, 1586−1592.

(21) Lai, A. L.; Millet, J. K.; Daniel, S.; Freed, J. H.; Whittaker, G. R. The SARS-CoV Fusion Peptide Forms an Extended Bipartite Fusion Platform That Perturbs Membrane Order in a Calcium-Dependent Manner. *J. Mol. Biol.* **2017**, *429*, 3875−3892.

(22) Birtles, D.; Lee, J. Identifying Distinct Structural Features of the SARS-CoV-2 Spike Protein Fusion Domain Essential for Membrane Interaction. *Biochemistry* **2021**, *60*, 2978−2986.

(23) Khelashvili, G.; Plante, A.; Doktorova, M.; Weinstein, H. Ca2+-Dependent Mechanism of Membrane Insertion and Destabilization by the SARS-CoV-2 Fusion Peptide. *Biophys. J.* **2021**, *120*, 1105−1119.

(24) Gorgun, D.; Lihan, M.; Kapoor, K.; Tajkhorshid, E. Binding Mode of SARS-CoV-2 Fusion Peptide to Human Cellular Membrane. *Biophys. J.* **2021**, *120*, 2914−2926.

(25) Koppisetti, R. K.; Fulcher, Y. G.; Van Doren, S. R. Fusion Peptide of SARS-CoV-2 Spike Rearranges into a Wedge Inserted in Bilayered Micelles. *J. Am. Chem. Soc.* **2021**, *143*, 13205−13211.

(26) Santamaria, A.; Batchu, K. C.; Matsarskaia, O.; Prévost, S. F.; Russo, D.; Natali, F.; Seydel, T.; Hoffmann, I.; Laux, V.; Haertlein, M.; Darwish, T. A.; Russell, R. A.; Corucci, G.; Fragneto, G.; Maestro, A.; Zaccai, N. R. Strikingly Different Roles of SARS-CoV-2 Fusion Peptides Uncovered by Neutron Scattering. *J. Am. Chem. Soc.* **2022**, *144*, 2968−2979.

(27) Shen, H.; Wu, Z.; Chen, L. Different Binding Modes of SARS-CoV-1 and SARS-CoV-2 Fusion Peptides to Cell Membranes: The

Influence of Peptide Helix Length. *J. Phys. Chem. B* **2022**, *126*, 4261−4271.
(28) Meher, G.; Chakraborty, H. Membrane Composition Modulates Fusion by Altering Membrane Properties and Fusion Peptide Structure. *J. Membr. Biol.* **2019**, *252*, 261−272.
(29) Meher, G.; Bhattacharjya, S.; Chakraborty, H. Membrane Cholesterol Modulates Oligomeric Status and Peptide-Membrane Interaction of Severe Acute Respiratory Syndrome Coronavirus Fusion Peptide. *J. Phys. Chem. B* **2019**, *123*, 10654−10662.
(30) Wang, S.; Li, W.; Hui, H.; Tiwari, S. K.; Zhang, Q.; Croker, B. A.; Rawlings, S.; Smith, D.; Carlin, A. F.; Rana, T. M. Cholesterol 25-Hydroxylase Inhibits SARS-CoV-2 and Other Coronaviruses by Depleting Membrane Cholesterol. *EMBO J.* **2020**, *39*, No. e106057.
(31) Kornhuber, J.; Hoertel, N.; Gulbins, E. The Acid Sphingomyelinase/Ceramide System in COVID-19. *Mol. Psychiatry* **2022**, *27*, 307−314.
(32) Mirabelli, C.; Wotring, J. W.; Zhang, C. J.; McCarty, S. M.; Fursmidt, R.; Pretto, C. D.; Qiao, Y.; Zhang, Y.; Frum, T.; Kadambi, N. S.; Amin, A. T.; O'Meara, T. R.; Spence, J. R.; Huang, J.; Alysandratos, K. D.; Kotton, D. N.; Handelman, S. K.; Wobus, C. E.; Weatherwax, K. J.; Mashour, G. A.; O'Meara, M. J.; Chinnaiyan, A. M.; Sexton, J. Z. Morphological Cell Profiling of SARS-CoV-2 Infection Identifies Drug Repurposing Candidates for COVID-19. *Proc. Natl. Acad. Sci. U.S.A.* **2021**, *118*, No. e2105815118.
(33) Gordon, D. E.; Jang, G. M.; Bouhaddou, M.; Xu, J.; Obernier, K.; White, K. M.; O'Meara, M. J.; Rezelj, V. V.; Guo, J. Z.; Swaney, D. L.; Tummino, T. A.; Hüttenhain, R.; Kaake, R. M.; Richards, A. L.; Tutuncuoglu, B.; Foussard, H.; Batra, J.; Haas, K.; Modak, M.; Kim, M.; Haas, P.; Polacco, B. J.; Braberg, H.; Fabius, J. M.; Eckhardt, M.; Soucheray, M.; Bennett, M. J.; Cakir, M.; McGregor, M. J.; Li, Q.; Meyer, B.; Roesch, F.; Vallet, T.; Mac Kain, A.; Miorin, L.; Moreno, E.; Naing, Z. Z. C.; Zhou, Y.; Peng, S.; Shi, Y.; Zhang, Z.; Shen, W.; Kirby, I. T.; Melnyk, J. E.; Chorba, J. S.; Lou, K.; Dai, S. A.; Barrio-Hernandez, I.; Memon, D.; Hernandez-Armenta, C.; Lyu, J.; Mathy, C. J. P.; Perica, T.; Pilla, K. B.; Ganesan, S. J.; Saltzberg, D. J.; Rakesh, R.; Liu, X.; Rosenthal, S. B.; Calviello, L.; Venkataramanan, S.; Liboy-Lugo, J.; Lin, Y.; Huang, X.-P.; Liu, Y.; Wankowicz, S. A.; Bohn, M.; Safari, M.; Ugur, F. S.; Koh, C.; Savar, N. S.; Tran, Q. D.; Shengjuler, D.; Fletcher, S. J.; O'Neal, M. C.; Cai, Y.; Chang, J. C. J.; Broadhurst, D. J.; Klippsten, S.; Sharp, P. P.; Wenzell, N. A.; Kuzuoglu-Ozturk, D.; Wang, H.-Y.; Trenker, R.; Young, J. M.; Cavero, D. A.; Hiatt, J.; Roth, T. L.; Rathore, U.; Subramanian, A.; Noack, J.; Hubert, M.; Stroud, R. M.; Frankel, A. D.; Rosenberg, O. S.; Verba, K. A.; Agard, D. A.; Ott, M.; Emerman, M.; et al. A SARS-CoV-2 Protein Interaction Map Reveals Targets for Drug Repurposing. *Nature* **2020**, *583*, 459−468.
(34) de Wilde, A. H.; Jochmans, D.; Posthuma, C. C.; Zevenhoven-Dobbe, J. C.; van Nieuwkoop, S.; Bestebroer, T. M.; van den Hoogen, B. G.; Neyts, J.; Snijder, E. J. Screening of an FDA-Approved Compound Library Identifies Four Small-Molecule Inhibitors of Middle East Respiratory Syndrome Coronavirus Replication in Cell Culture. *Antimicrob. Agents Chemother.* **2014**, *58*, 4875−4884.
(35) Tessier, C.; Nuss, P.; Staneva, G.; Wolf, C. Modification of Membrane Heterogeneity by Antipsychotic Drugs: An X-Ray Diffraction Comparative Study. *J. Colloid Interface Sci.* **2008**, *320*, 469−475.
(36) McNew, J. A.; Weber, T.; Parlati, F.; Johnston, R. J.; Melia, T. J.; Söllner, T. H.; Rothman, J. E. Close Is Not Enough: SNARE-Dependent Membrane Fusion Requires an Active Mechanism That Transduces Force to Membrane Anchors. *J. Cell Biol.* **2000**, *150*, 105−118.
(37) Daste, F.; Sauvanet, C.; Bavdek, A.; Baye, J.; Pierre, F.; Le Borgne, R.; David, C.; Rojo, M.; Fuchs, P.; Tareste, D. The Heptad Repeat Domain 1 of Mitofusin Has Membrane Destabilization Function in Mitochondrial Fusion. *EMBO Rep.* **2018**, *19*, No. e43637.
(38) Scott, B. L.; Van Komen, J. S.; Liu, S.; Weber, T.; Melia, T. J.; McNew, J. A. Liposome Fusion Assay to Monitor Intracellular Membrane Fusion Machines. *Meth. Enzymol.* **2003**, *372*, 274−300.
(39) Ingólfsson, H. I.; Carpenter, T. S.; Bhatia, H.; Bremer, P.-T.; Marrink, S. J.; Lightstone, F. C. Computational Lipidomics of the Neuronal Plasma Membrane. *Biophys. J.* **2017**, *113*, 2271−2280.
(40) Düzgüneş, N.; Wilschut, J.; Fraley, R.; Papahadjopoulos, D. Studies on the Mechanism of Membrane Fusion. Role of Head-Group Composition in Calcium- and Magnesium-Induced Fusion of Mixed Phospholipid Vesicles. *Biochim. Biophys. Acta* **1981**, *642*, 182−195.
(41) Nir, S.; Wilschut, J.; Bentz, J. The Rate of Fusion of Phospholipid Vesicles and the Role of Bilayer Curvature. *Biochim. Biophys. Acta* **1982**, *688*, 275−278.
(42) Malinin, V. S.; Frederik, P.; Lentz, B. R. Osmotic and Curvature Stress Affect PEG-Induced Fusion of Lipid Vesicles but Not Mixing of Their Lipids. *Biophys. J.* **2002**, *82*, 2090−2100.
(43) Lee, J. Y.; Schick, M. Calculation of Free Energy Barriers to the Fusion of Small Vesicles. *Biophys. J.* **2008**, *94*, 1699−1706.
(44) Seeman, P.; Lee, T. Antipsychotic Drugs: Direct Correlation between Clinical Potency and Presynaptic Action on Dopamine Neurons. *Science* **1975**, *188*, 1217−1219.
(45) Wisniewska, A.; Wolnicka-Glubisz, A. ESR Studies on the Effect of Cholesterol on Chlorpromazine Interaction with Saturated and Unsaturated Liposome Membranes. *Biophys. Chem.* **2004**, *111*, 43−52.
(46) Jutila, A.; Söderlund, T.; Pakkanen, A. L.; Huttunen, M.; Kinnunen, P. K. Comparison of the Effects of Clozapine, Chlorpromazine, and Haloperidol on Membrane Lateral Heterogeneity. *Chem. Phys. Lipids* **2001**, *112*, 151−163.
(47) Hughes, Z. E.; Mark, A. E.; Mancera, R. L. Molecular Dynamics Simulations of the Interactions of DMSO with DPPC and DOPC Phospholipid Membranes. *J. Phys. Chem. B* **2012**, *116*, 11911−11923.
(48) Kapoor, R.; Peyear, T. A.; Koeppe, R. E.; Andersen, O. S. Antidepressants Are Modifiers of Lipid Bilayer Properties. *J. Gen. Physiol.* **2019**, *151*, 342−356.
(49) Zidovetzki, R.; Levitan, I. Use of Cyclodextrins to Manipulate Plasma Membrane Cholesterol Content: Evidence, Misconceptions and Control Strategies. *Biochim. Biophys. Acta* **2007**, *1768*, 1311−1324.
(50) Lavieu, G.; Scarlatti, F.; Sala, G.; Carpentier, S.; Levade, T.; Ghidoni, R.; Botti, J.; Codogno, P. Regulation of Autophagy by Sphingosine Kinase 1 and Its Role in Cell Survival during Nutrient Starvation. *J. Biol. Chem.* **2006**, *281*, 8518−8527.
(51) Qing, E.; Kicmal, T.; Kumar, B.; Hawkins, G. M.; Timm, E.; Perlman, S.; Gallagher, T. Dynamics of SARS-CoV-2 Spike Proteins in Cell Entry: Control Elements in the Amino-Terminal Domains. *mBio* **2021**, *12*, No. e0159021.
(52) Birtles, D.; Oh, A. E.; Lee, J. Exploring the PH Dependence of the SARS-CoV-2 Complete Fusion Domain and the Role of Its Unique Structural Features. *Protein Sci.* **2022**, *31*, No. e4390.
(53) Zhou, T.; Tsybovsky, Y.; Gorman, J.; Rapp, M.; Cerutti, G.; Chuang, G.-Y.; Katsamba, P. S.; Sampson, J. M.; Schön, A.; Bimela, J.; Boyington, J. C.; Nazzari, A.; Olia, A. S.; Shi, W.; Sastry, M.; Stephens, T.; Stuckey, J.; Teng, I.-T.; Wang, P.; Wang, S.; Zhang, B.; Friesner, R. A.; Ho, D. D.; Mascola, J. R.; Shapiro, L.; Kwong, P. D. Cryo-EM Structures of SARS-CoV-2 Spike without and with ACE2 Reveal a PH-Dependent Switch to Mediate Endosomal Positioning of Receptor-Binding Domains. *Cell Host Microbe* **2020**, *28*, 867−879.e5.
(54) Sanders, D. W.; Jumper, C. C.; Ackerman, P. J.; Bracha, D.; Donlic, A.; Kim, H.; Kenney, D.; Castello-Serrano, I.; Suzuki, S.; Tamura, T.; Tavares, A. H.; Saeed, M.; Holehouse, A. S.; Ploss, A.; Levental, I.; Douam, F.; Padera, R. F.; Levy, B. D.; Brangwynne, C. P. SARS-CoV-2 Requires Cholesterol for Viral Entry and Pathological Syncytia Formation. *eLife* **2021**, *10*, No. e65962.
(55) Baier, C. J.; Barrantes, F. J. Role of Cholesterol-Recognition Motifs in the Infectivity of SARS-CoV-2 Variants. *Colloids Surf. B Biointerfaces* **2023**, *222*, 113090.
(56) Sostarecz, A. G.; McQuaw, C. M.; Ewing, A. G.; Winograd, N. Phosphatidylethanolamine-Induced Cholesterol Domains Chemically Identified with Mass Spectrometric Imaging. *J. Am. Chem. Soc.* **2004**, *126*, 13882−13883.

https://doi.org/10.1021/acsomega.3c03610
ACS Omega 2023, 8, 32729−32739

(57) Yang, S.-T.; Kiessling, V.; Simmons, J. A.; White, J. M.; Tamm, L. K. HIV Gp41-Mediated Membrane Fusion Occurs at Edges of Cholesterol-Rich Lipid Domains. *Nat. Chem. Biol.* **2015**, *11*, 424−431.
(58) Carpinteiro, A.; Gripp, B.; Hoffmann, M.; Pöhlmann, S.; Hoertel, N.; Edwards, M. J.; Kamler, M.; Kornhuber, J.; Becker, K. A.; Gulbins, E. Inhibition of Acid Sphingomyelinase by Ambroxol Prevents SARS-CoV-2 Entry into Epithelial Cells. *J. Biol. Chem.* **2021**, *296*, 100701.
(59) Dyall, J.; Coleman, C. M.; Hart, B. J.; Venkataraman, T.; Holbrook, M. R.; Kindrachuk, J.; Johnson, R. F.; Olinger, G. G.; Jahrling, P. B.; Laidlaw, M.; Johansen, L. M.; Lear-Rooney, C. M.; Glass, P. J.; Hensley, L. E.; Frieman, M. B. Repurposing of Clinically Developed Drugs for Treatment of Middle East Respiratory Syndrome Coronavirus Infection. *Antimicrob. Agents Chemother.* **2014**, *58*, 4885−4893.
(60) Plaze, M.; Attali, D.; Prot, M.; Petit, A.-C.; Blatzer, M.; Vinckier, F.; Levillayer, L.; Chiaravalli, J.; Perin-Dureau, F.; Cachia, A.; Friedlander, G.; Chrétien, F.; Simon-Loriere, E.; Gaillard, R. Inhibition of the Replication of SARS-CoV-2 in Human Cells by the FDA-Approved Drug Chlorpromazine. *Int. J. Antimicrob. Agents* **2021**, *57*, 106274.
(61) Xia, S.; Yan, L.; Xu, W.; Agrawal, A. S.; Algaissi, A.; Tseng, C.-T. K.; Wang, Q.; Du, L.; Tan, W.; Wilson, I. A.; Jiang, S.; Yang, B.; Lu, L. A Pan-Coronavirus Fusion Inhibitor Targeting the HR1 Domain of Human Coronavirus Spike. *Sci. Adv.* **2019**, *5*, No. eaav4580.
(62) Xia, S.; Liu, M.; Wang, C.; Xu, W.; Lan, Q.; Feng, S.; Qi, F.; Bao, L.; Du, L.; Liu, S.; Qin, C.; Sun, F.; Shi, Z.; Zhu, Y.; Jiang, S.; Lu, L. Inhibition of SARS-CoV-2 (Previously 2019-NCoV) Infection by a Highly Potent Pan-Coronavirus Fusion Inhibitor Targeting Its Spike Protein That Harbors a High Capacity to Mediate Membrane Fusion. *Cell Res.* **2020**, *30*, 343−355.
(63) Yang, K.; Wang, C.; Kreutzberger, A. J. B.; Ojha, R.; Kuivanen, S.; Couoh-Cardel, S.; Muratcioglu, S.; Eisen, T. J.; White, K. I.; Held, R. G.; Subramanian, S.; Marcus, K.; Pfuetzner, R. A.; Esquivies, L.; Doyle, C. A.; Kuriyan, J.; Vapalahti, O.; Balistreri, G.; Kirchhausen, T.; Brunger, A. T. Nanomolar Inhibition of SARS-CoV-2 Infection by an Unmodified Peptide Targeting the Prehairpin Intermediate of the Spike Protein. *Proc. Natl. Acad. Sci. U.S.A.* **2022**, *119*, No. e2210990119.
(64) de Vries, R. D.; Schmitz, K. S.; Bovier, F. T.; Predella, C.; Khao, J.; Noack, D.; Haagmans, B. L.; Herfst, S.; Stearns, K. N.; Drew-Bear, J.; Biswas, S.; Rockx, B.; McGill, G.; Dorrello, N. V.; Gellman, S. H.; Alabi, C. A.; de Swart, R. L.; Moscona, A.; Porotto, M. Intranasal Fusion Inhibitory Lipopeptide Prevents Direct-Contact SARS-CoV-2 Transmission in Ferrets. *Science* **2021**, *371*, 1379−1382.

https://doi.org/10.1021/acsomega.3c03610
ACS Omega 2023, 8, 32729−32739